

Intelligent-Tire-Based Slip Ratio Estimation Using Machine Learning

Nan Xu, Zepeng Tang, Jianfeng Zhou, Hassan Askari

Abstract—Autonomous vehicles are most concerned about safety control issue, and slip ratio is critical to the safety of the vehicle control system. In this paper, different machine learning algorithms (Neural Networks, Gradient Boosting Machine, Random Forest, and Support Vector Machine) are used to train the slip ratio estimation model based on the acceleration signals (a_x , a_y , and a_z) from the tri-axial Micro-Electro Mechanical System (MEMS) accelerometer utilized in the intelligent tire system, where the acceleration signals are divided into four sets ($a_x/a_y/a_z$, a_x/a_z , a_y/a_z , and a_z) as algorithm inputs. The experimental data used in this study are collected through the MTS Flat-Trac tire test platform. Performance of different slip ratio estimation models is compared using the NRMS errors in 10-fold cross-validation (CV). The results indicate that NN and GBM have more promising accuracy, and the a_z input type has better performance compared to other input types, with the best result being the estimation model of the NN algorithm with a_z as input, which results is 4.88%. The present study with the fusion of intelligent tire system and machine learning paves the way for the accurate estimation of tire slip ratio under different driving conditions, which will open up a new way of Autonomous vehicles, intelligent tires, and tire slip ratio estimation.

Index Terms—Intelligent tire, tire slip ratio estimation, machine learning, vehicle system dynamics, sensing systems.

I. INTRODUCTION

AUTONOMOUS vehicles are going through a rapid development stage and are becoming more and more popular. Current the major concern is how to ensure effective safety control in autonomous vehicles that are removed from the driver's control [1], [2]. The slip ratio is a key factor affecting the safety and stability of the vehicle's traction control system [3]. Excessive slip ratio may reduce the braking ability, in addition to the loss of steering ability if the front wheels lose lateral adhesion, and if the rear wheels lose lateral adhesion, safety risks such as sideslip may happen. Therefore, the slip ratio needs to be effectively controlled. For example, the Anti-lock Braking System (ABS) [4] and Traction Control System (TCS) [5] that have been developed are used to ensure that the tires have optimal traction by limiting the tire slip ratio to

This work has been submitted to the IEEE for possible publication. Copyright may be transferred without notice, after which this version may no longer be accessible. This research is supported by National Natural Science Foundation of China (Grant Nos.51875236 and 61790561), China Automobile Industry Innovation.

N. Xu, Z. Tang and J. Zhou are with the State Key Laboratory of Automotive Simulation and Control, Jilin University, Changchun, Jilin, 130025, China and N. Xu is also with the Department of Mechanical and Mechatronics Engineering, University of Waterloo, ON. N2L3G1, Canada, e-mail: (xunan@jlu.edu.cn, tangzp19@mails.jlu.edu.cn, and zhoujf20@mails.jlu.edu.cn).

H. Askari is at the Department of Mechanical and Mechatronics Engineering, University of Waterloo, ON. N2L3G1, Canada e-mail: (h2askari@uwaterloo.ca, and a.khajepour@uwaterloo.ca)

an effective range. It can be derived from Equation 1 that the slip ratio (κ), as observed in Fig. 1, mainly reflects the rate of the difference between the longitudinal vehicle speed (V_x) and the wheel velocity (V_w), i.e., the level of slip of the tire relative to the road.

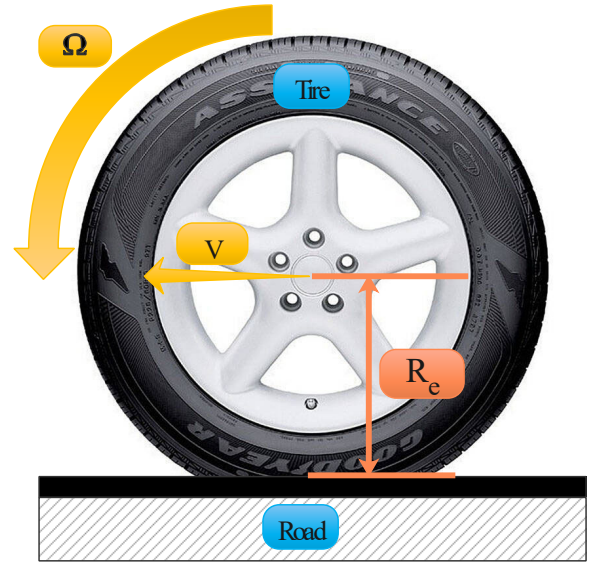


Fig. 1: Schematic representation of a tire interacting with road

$$\kappa = \frac{V_w - V_x}{V_x} = \frac{\Omega R_e - V_x}{V_x} \times 100\% \quad (1)$$

where V_w and V_x are wheel velocity and longitudinal velocity of vehicle, respectively. Ω is wheel angular velocity and R_e is the tire effective radius.

The existing slip ratio estimation methods can be divided into two categories according to the signals used, one using V_x combined with Ω to calculate, and the other main category choosing alternative signals, such as vehicle longitudinal acceleration (A_x) or electric vehicle drive torque (T), together with Ω to calculate. There are differences in the specific methods of these two categories. For example, in the method of estimating the slip ratio based on V_x , where the most fundamental issue and an area of current academic interest is how to accurately estimate V_x . The existing ones have been developed based on Kalman Filter (KF) [6], Extended Kalman Filter (EKF) [7], Unscented Kalman Filter (UKF) [3] and sliding mode observer (SMO) [8], [9] to establish state space equations for estimating V_x , but all of these V_x estimation methods are actually more complicated and have

accuracy errors, which causes the cumulative errors in the results of this method of calculating slip ratio based on V_x . In addition, there are GPS/INS sensors used to measure V_x , but in urban environments or tunnels, etc., V_x measurement may suffer from failures [10].

And another main category in the method of estimating the slip ratio without using V_x , Hori et al. in 1998 used V_w of the non-driven wheel instead of V_x to estimate the slip ratio because V_x is not easily available [11]. And later, Fujii et al. proposed to build the state equation to estimate the slip ratio by using the easily available T and Ω of electric vehicles in 2007 [12], and in addition, it's methods required parameters such as tire inertia and vehicle mass. In 2012, Cecotti et al. added a small cosine signal to T , which resulted in small variations in Ω as well, and measured these variations to obtain the phase shift and gain relative to the torque oscillation, thus the slip ratio was estimated based on the transfer function between Ω and T [13]. However, the results of this method are more sensitive to the frequency of the added signal. A similar approach based on T was also used by Boisvert et al. [7], who used the EKF to model the nonlinearity between slip ratio and T to calculate slip ratio in 2016. In addition, there are also studies that apply acceleration signals obtained from on-board sensors, such as Maeda et al. [14] and Vo-Duy et al. [15], who established a state estimation equation between the A_x obtained from on-board acceleration sensors and the Ω obtained from electric vehicles to calculate the slip ratio.

To summarize the two traditional methods of estimating slip ratio, there are still some problems. The first aspect is due to the use of a large number of parameters, such as vehicle mass and wheel rotational inertia, and the variation of these variables may affect the estimation performance. The second aspect is that the estimation model uses a rather large state vector, and thus the method is complex and computationally intensive, which poses a challenge for real-time performance. The third aspect is that additional on-board sensors, such as acceleration sensors, wheel speed sensors, etc., are used, which make it difficult to meet the real-time estimation requirements of the estimator due to the low update frequency, while the noise from multiple sources of sensors can cause accumulation to make the estimation results vary or even unstable. However, with the coming of the era of autonomous vehicles, more and more advanced sensors are entering the automotive industry, such as the development of intelligent tires in recent years provides us with a new idea to acquire signals directly through sensors installed in the inner liner of tire and extract relevant features from them to establish a relationship with tire state parameters, so that only through the signal measured by the sensors in the tire can calculate the required tire state. Thus, the above problems can be improved. First, no additional vehicle parameters are used, and the sources of factors affecting the estimation performance are reduced. Second, the estimation model can use only the sensor signals from the tire, and the computational effort is relatively reduced. Third, no additional sensors are used, and the error accumulation of multiple source sensors is avoided.

So far, intelligent tires have been developed for several years, during this period many types of sensors have been used

inside the tire to monitor acceleration, strain or deformation in the tire contact patch, such as Micro-Electro-Mechanical System (MEMS) acceleration sensors [16], [17] for measuring acceleration, and stress sensors [18], [19], triboelectric nanogenerator (TENG) [20], [21], capacitive sensors [22], [23], optical fiber sensors [24], [25], surface acoustic wave sensors [26], [27] and magnetic sensors [28] for measuring strain, and optical sensors [29] and ultrasonic distance sensors [30] for measuring the relative distance of the tire tread to the rim, i.e., the global deformation. Meanwhile, researchers have made many contributions in the field of state parameter estimation by applying intelligent tire technology, such as tire force [16], tire slip angle [17], road friction coefficient [31], [32], and so on. While in the area of tire slip ratio, there is no research work related to intelligent tires found yet. The MEMS acceleration sensor is selected as the sensor for this study to explore the performance of intelligent tires in slip ratio estimation.

In this paper, the acceleration signals generated by the intelligent tire system are collected by an National Instrument (NI) data acquisition system (DAQ), and used for data analysis and pre-processing. The data analysis is performed to investigate the correlation between acceleration signals and slip ratio in three directions, while the data pre-processing process consists of filtering, extraction of acceleration signals around the center of the contact patch and data normalization. Subsequently, four sets of acceleration signals are used as input to the machine learning, with four sets of longitudinal (a_x) / lateral (a_y) / vertical (a_z) acceleration, a_x/a_z , a_y/a_z , and a_z . Also, in order to more widely verify and evaluate the performance of machine learning algorithms based on intelligent tires in slip ratio estimation, four machine learning algorithms are tested for comparison, which include Neural Network (NN), Gradient Boosting Machine (GBM), Random Forest (RF), and Support Vector Machine (SVM).

The framework of this paper is organized as follows. Section II introduces the test system as well as the design of the working conditions, where the test system includes the Measure Test Simulate (MTS) tire test system and the intelligent tire system. Section III analyzes the acceleration signal to extract the features related to the slip ratio. Section IV presents the pre-processing of the data to prepare for the modeling of the machine learning algorithms. Section V comprehensively analyzes and discusses the estimation results of the machine learning algorithms using four input types for the slip ratio, respectively, and provides a 10-fold cross-validation (CV) validation of the four algorithms and four inputs. Finally, the conclusions and future research work of this paper are stated.

II. TEST AND SIGNAL ACQUISITION

The entire test system can be regarded as two systems, which are the Measure Test Simulate (MTS) tire test system and the intelligent tire system. The MTS tire test system is used to set up different scenarios and collect data such as slip ratio, slip angle, tire forces, etc., while collecting acceleration sensor signals is based on the intelligent tire system. The whole test system is shown in Fig. 2, and the details of which are presented in this section.

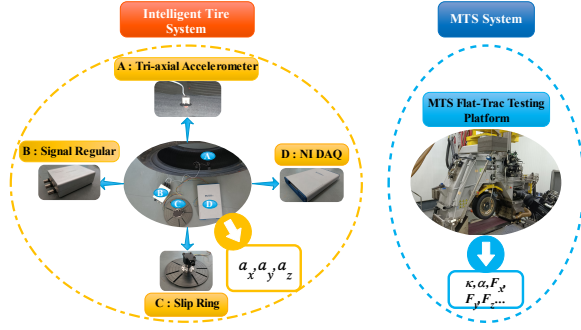


Fig. 2: The entire test system

A. MTS Tire Experimental System

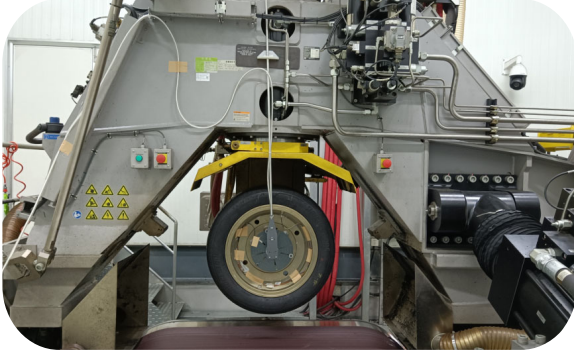


Fig. 3: MTS tire testing platform

To get the data with slip ratio, the MTS Flat-Trac tire test system (Fig. 3) is applied to conduct different experiments, which can also obtain data on tire longitudinal force (F_x), lateral force (F_y), vertical force (F_z), slip angle (α), and slip ratio (κ), etc. These data can subsequently be provided to validate the results of the intelligent tire estimation.

B. Intelligent Tire System

The intelligent tire system in this article consists of a Micro-electro mechanical Systems (MEMS) tri-axial acceleration sensor, a high-speed slip ring, a signal regulator, and an National Instrument (NI) data acquisition system (DAQ), as shown in Fig. 2.

The tri-axial acceleration sensor is glued the inner liner of the tire to measure the three direction acceleration signals (a_x , a_y , and a_z) generated in the tire contact patch in Fig. 4a, and the definition of its coordinates system orientation is shown in Fig. 4b. The signal wire then passes through the valve nozzle through the rim, see Fig. 5a, where the valve nozzle device is sealed with sealant to avoid tire air leakage. After exiting the rim, it has to pass through the high-speed slip ring in Fig. 5b, this is a 6-channel slip ring made by Michigan Scientific, which is designed to be mounted on the rim and used to transmit the acceleration signal from the rotating tire to the NI DAQ system. The signal regulator uses three channels (corresponding to the three acceleration directions) to provide a constant current source to supply power the accelerometer. The NI DAQ system can be used to collect the

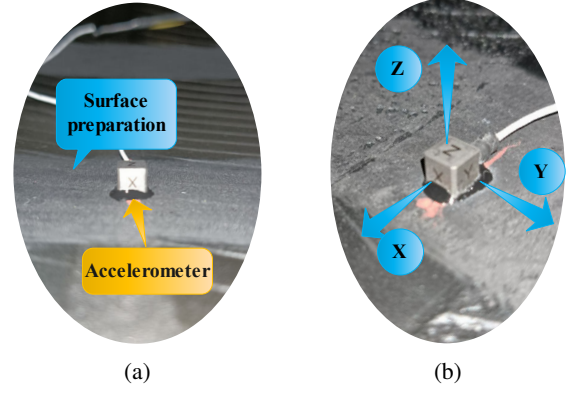


Fig. 4: (a) Installation of accelerometer in tire; (b) Coordinate system of accelerometer in tire

acceleration signal by adjusting the signal channels, sampling frequency and sampling method (differential mode or single-ended reference mode). The single-ended reference mode (selected when the signal regulator is grounded) is adopted for this test, and the sampling frequency is chosen to be 10 KHz, which is adequate to meet the research requirements.

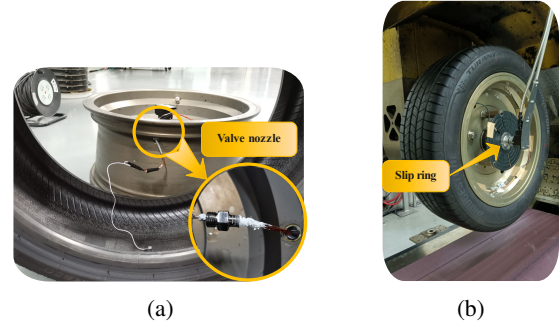


Fig. 5: (a) Using the valve nozzle across the rim; (b) Transferred via slip ring

C. Test Scenarios

This experiment is conducted using Bridgestone tires for testing, and three loads, two velocities and different slip ratios are changed respectively. There are two main types according to the variation of the slip ratio, one is that the slip ratio remains constant at specific values during some tire rotations, which increases progressively from -4% to +4% (Data set 1). The other is that the slip ratio varies continuously in a triangular wave manner during tire rotations, a part of which is the small continuous slip ratio (Data set 2), its alteration follows the 0-(-3%)-3%-0 rule, and the remaining part is the large continuous slip ratio (Data set 3), the varying law is 0-(-30%)-30%-0. In total, the experimental data of 2218 tire revolutions (1082 in Data set 1, 666 in Data set 2, and 470 in Data set 3) is used to develop the different machine learning based tire slip ratio algorithm, and each of them is divided into training (70%) and testing datasets (30%).

TABLE I: TESTING SCENARIOS

Driving/braking	Parameters
Tire brand	Bridgestone 215/55R17
Pressure [kPa]	250
Vertical load [N]	2680,4020,5360
Velocity [km/h]	30,60
Slip ratio [%]	$\pm 4, \pm 3, \pm 2, \pm 1$, Triangular wave(3 and up to 30)

III. DATA ANALYSIS

In this section, the acceleration signals in three directions (a_x, a_y , and a_z) of longitudinal slip conditions are analyzed in detail trying to find the correlation characteristics between the acceleration signals and the slip ratio. The acceleration signals shown in the following are $\pm 35^\circ$ from the center of the tire contact patch (the method of determining tire contact patch is presented in section IV), which are processed by 400Hz Butter-worth low-pass filtering [16].

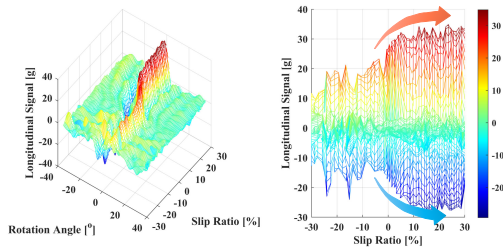


Fig. 6: Longitudinal acceleration in time domain in Data set 3 (60km/h at 2680N load)

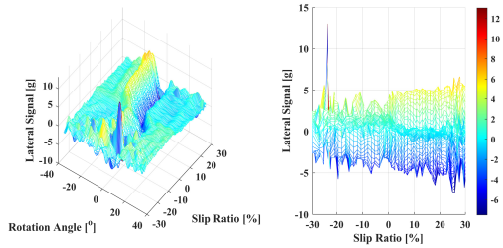


Fig. 7: Lateral acceleration in time domain in Data set 3 (60km/h at 2680N load)

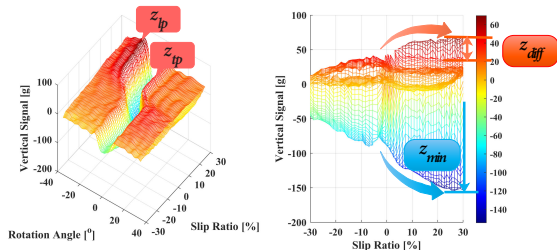


Fig. 8: Vertical acceleration in time domain in Data set 3 (60km/h at 2680N load)

Figs. 6-8 show the a_x , a_y and a_z signals for Data set 3, respectively. Each plot consists of two subplots, the left plot is a 3D view and the right plot is a side view of the x-axis slip

ratio. From Fig. 6, it can be observed that the a_x will show two peaks when entering and leaving the tire contact patch, where the peak change decreases and then increases. At the same time, these two peaks have some correlation with the slip ratio, it can be found from the right subplot that the absolute values of the maximum and minimum values of the a_x increase simultaneously when the slip ratio changes to the positive slip ratio, which shows nonlinearity. On the negative slip ratio, the peak change of the a_x is not very obvious. In Fig. 7, the a_y signal, when entering and leaving the tire contact patch, changes in the opposite order to the a_x , showing increasing first and then decreasing. However, the correlation between the peak of the a_y and slip ratio is not found from the right subplot. In Fig. 8, the a_z is most clearly characterized by the low center and high sides, where the lowest value in the center is labeled as z_{min} and the high side values are labeled as z_{lp} and z_{tp} respectively according to the leading peak and trailing peak of the tire contact patch. As can be observed in the left subplot, the color of the left and right peaks varies at different slip ratios, described in a more detailed way as a greater acceleration of z_{tp} relative to z_{lp} at negative slip ratio, and a greater value of z_{lp} than z_{tp} at positive slip ratio. This feature is characterized by z_{diff} , which represents the magnitude of the difference between z_{lp} and z_{tp} . In addition to this, it can also be noticed from the subplot on the right that the value of z_{min} decreases from -30% to 30% slip ratio, and intuitively the value of z_{min} shows a similar linear variation with respect to the slip ratio of the x-axis.

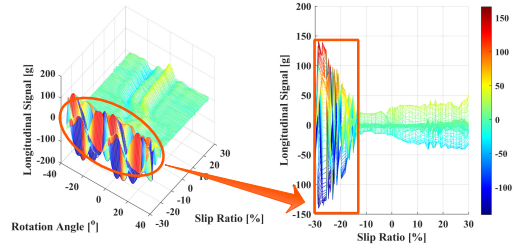


Fig. 9: Longitudinal acceleration in time domain in Data set 3 (60km/h at 4020N load)

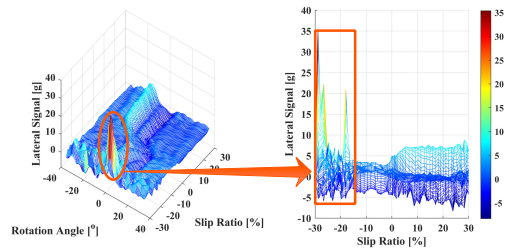


Fig. 10: Lateral acceleration in time domain in Data set 3 (60km/h at 4020N load)

The features observed above are presented using 60km/h at 2680N. In order to find more accurate and reliable features, acceleration signals at more working conditions need to be analyzed, such as the acceleration signal under 60km/h at 4020N shown in Figs. 9-11. In Figs. 9 and 10, it can be found

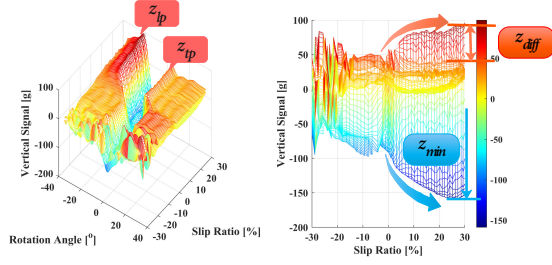


Fig. 11: Vertical acceleration in time domain in Data set 3 (60km/h at 4020N load)

that in the negative slip ratio region, the a_x and a_y signals show anomalous values after the slip ratio is below about -15%. The reason for this is thought to be, on the one hand, that the filter cutoff frequency may be set too high, leading to noise interference, and on the other hand, that the acceleration signal itself has lost its significance under such working conditions. While the a_x and a_y signals gradually show anomalous values, what is of more interest is that the a_z always maintains a very promising characteristic in Fig. 11. In the experimental data of this study (TABLE I), the acceleration signals in three directions for all working conditions at 30 km/h are consistent with the characteristics observed in Figs. 6-8, and no outliers appear. For the working conditions at 60 km/h, except for the a_z , which has always maintained a stable characteristic, the a_x and a_y show abnormal values under the loads of 4020 N and 5360 N. In summary, the a_z showed more stable and reliable characteristics in all the experimental conditions, so in order to further observe the a_z , the above z_{diff} and z_{min} are counted and plotted for analysis, as shown in Figs. 12 and 13.

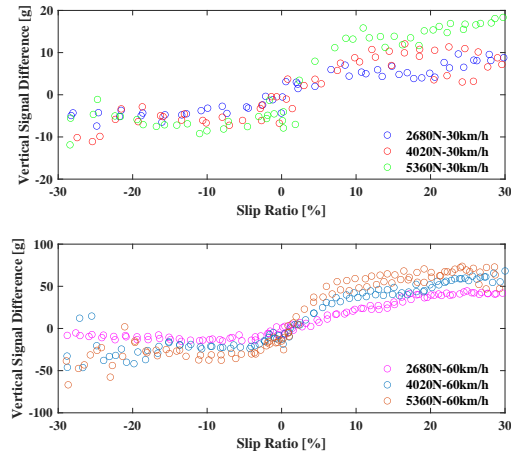


Fig. 12: Variation of vertical signal difference with slip ratio under different working conditions

The variation curve of z_{diff} vs. slip ratio is shown in Fig. 12, and different colors represent different working conditions as shown in the legend of the figure. In the region of slip ratio between about -8% and 8%, the value of z_{diff} grows linearly, and when the absolute value of slip ratio exceeds 8%, the value of z_{diff} tends to saturate and the growth

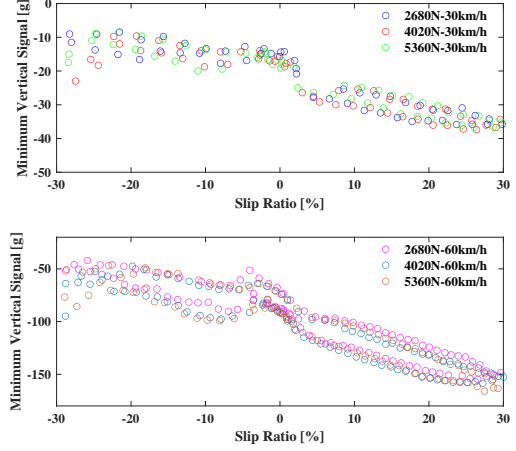


Fig. 13: Variation of minimum vertical signal with slip ratio under different working conditions

rate gradually slows down, showing a non-linear variation relationship overall. This feature is very similar to the tire mechanical properties [33], [34] and can be used to estimate the longitudinal tire force in future research work. The absolute value of z_{diff} shows that it is larger at positive slip ratio than at negative slip ratio, which is consistent with what is observed in the left subplot in Figs. 8 and 11. Fig. 13 shows the variation curves of z_{min} and slip ratio, both of which have a relatively simpler and more linear change in the general. The value of z_{min} keeps decreasing as the slip ratio increases. There is also an interesting feature, which is clearly observable similar to the hysteresis phenomenon that occurs in the mechanical properties of the tire [35]. From the results of the above analysis, the correlation between slip ratio and acceleration signals in the three directions can be expressed as, $a_z > a_x \sim a_y$.

IV. METHODOLOGY

The more important part of machine learning algorithm is the pre-processing of data, which influences the result of the algorithm. In order to make the model simpler and more effective, dataset size should be minimized as much as possible while ensuring its primary features. Meanwhile, the hyper-parameters of the machine learning algorithm used in this paper are described in detail below.

A. Data Pre-Processing

In the acceleration signal pre-processing, the signal in the tire contact patch is of utmost importance. In the following, we will present how to extract the acceleration signal in the tire contact patch and select proper sample points to train the machine learning algorithm. The data pre-processing process is mainly divided into filtering, identifying the tire contact patch signal, and data normalization. The whole process is as shown in Fig. 14.

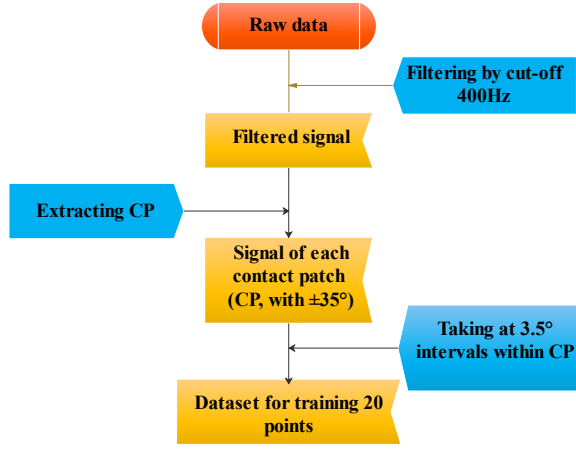


Fig. 14: Flowchart of data pre-processing

1) *Filtering*: The data acquired by the DAQ system at 10 kHz is sampled for spectral analysis. In this paper, 400 Hz is chosen as the cutoff frequency for this Butterworth low-pass filtering, since this part is mainly caused by tire deformation [16].

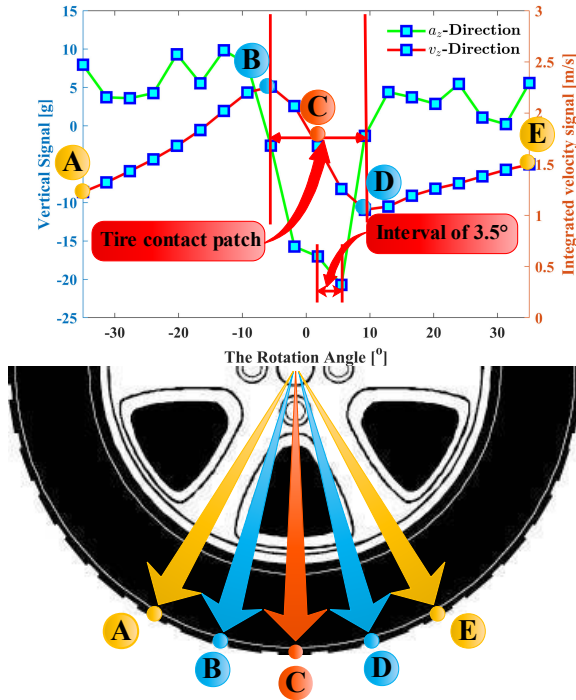


Fig. 15: Determining sample points in the contact patch

2) *Extracting the contact patch*: Due to the serious deformation of the a_x under longitudinal slip conditions (as described previously in Fig. 9), the method of determining the contact patch according to the leading and trailing peaks of the a_x is no longer applicable [16], and the integrated value of a_z , i.e., the vertical velocity (v_z), is used here to determine the contact patch. As shown in Fig. 15, it can be clearly seen that there are two peaks in the v_z when the sensor enters and leaves the contact patch. At the same time, the rotation angle of the tire is recorded by the encoder to accurately locate

the position of the acceleration sensor. The two peaks of the v_z (points B and D, respectively) are observed to correspond to about $\pm 10^\circ$ of the encoder, and the acceleration signal at $\pm 35^\circ$ is extracted in order to provide the machine learning algorithm with more information about the acceleration in the contact patch (it corresponds to points A and E). On the other hand, the number of sampling points changes with the increase of the Ω , so training samples can be captured according to the tire rotation angle. Meanwhile, in order to make the machine learning algorithm computationally efficient, a sample point is extracted at each 3.5° interval [17], while being able to ensure the acceleration information within the basic contact patch. That is, each rotation of the tire can generate 20 sample points to be utilized as input to the algorithm.

3) *Data normalization*: In order to enable the data to achieve fast convergence in machine learning algorithms, such as NN, GBM, and SVM, it is necessary to normalize the data, and the Min-Max normalization method is employed in this work as follows:

$$x_{norm} = \frac{x - x_{min}}{x_{max} - x_{min}} \quad (2)$$

where x presents the measured data, x_{min} and x_{max} are the minimum and maximum of the acquired data. Note that, RF does not require data normalization process.

B. Machine Learning Methods Training

Within the field of state parameter estimation of vehicles and tires, the current predominantly used machine learning methods are Decision Tree algorithms (Decision Tree, Random Forest, Gradient Boosting Machine, etc.), Neural Network family (Artificial Neural Network, Convolutional Network, Recurrent Neural Network, etc.), and Support Vector Machine [16], [17]. And each single algorithm has its own pros and cons for all possible data sets, so in this paper, four commonly used algorithms, Artificial Neural Network (ANN), Gradient Boosting Machine (GBM), Random Forest (RF), and Support Vector Machine (SVM) are employed to investigate and evaluate the results of estimation of slip ratio.

NN mainly consist of an input layer, a hidden layer (one or more layers) and an output layer. It can obtain a deeper model representation by increasing the number of hidden layers. The NN based on the Resilient backpropagation (Rprop) algorithm [21] is used in this case because Rprop can effectively solve noise errors and is more suitable for hardware applications [36]. GBM is a method for regression and classification that combines weak learners into one strong learner by iterative methods [37]. Both RF and GBM belong to the class of decision trees, and compared to GBM, RF are easier to train and less prone to over-fitting. In practical application, RF have proven to be a very effective method, but for processing regressions that do not go beyond the range of target values in which they are trained [38]. SVM can be used for classification and regression analysis. In solving the case of linearly indistinguishable data, it is achieved mainly by applying the kernel function technique, by mapping the vectors to a higher dimensional space, establishing a maximally interval hyperplane, and building two critical hyperplanes parallel to

each other on both sides of the hyperplane that separates the data, and the greater the distance between the two critical hyperplanes, the smaller the total error of the classifier [39].

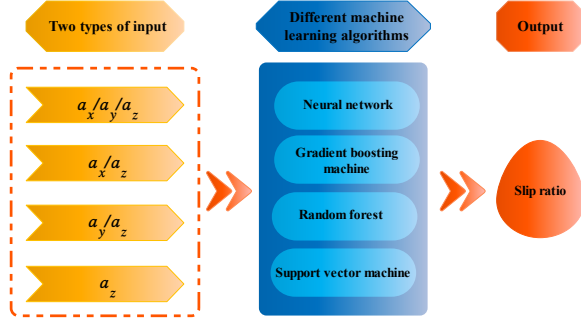


Fig. 16: Diagram of the input and output of different machine learning algorithms

Four categories are used as input to machine learning in this research, which are $a_x/a_y/a_z$, a_x/a_z , a_y/a_z , and a_z . The output of all machine learning algorithms is the slip ratio, as shown in Fig. 16. This research work is based on R software platform computing and uses four machine learning algorithms as a comparison analysis. All training datasets in this research were conducted on a laptop computer with Intel(R) Core(TM) i5-10200H CPU @2.4GHz and 16GB of DDR4 RAM. The hyper-parameters used for all models were assigned by "trial and error" method. The NN is based on the Rprop algorithm for slip ratio estimation, and its hidden layer is 10-5-1. The hyper-parameters of the GBM are as follows: trees = 4295, interaction.depth = 3, shrinkage = 0.1, n.minobinnode = 10, and bag.fraction = 1. The tree of RF is chosen to be 50. The gamma of SVM is set to 0.0312 and cost is 32. Four categories of inputs are used with the same hyper-parameters as above.

V. RESULTS AND DISCUSSIONS

This section is composed of two main parts. Firstly, the results of slip ratio estimation based on various machine learning algorithms with four inputs are shown and presented for four working conditions, which are Data set 1, Data set 2, Data set 3 and Data set 4 respectively, where Data set 4 is the collection of Data set 1, Data set 2, and Data set 3. Secondly, in order to carry out more convincing evidence, the 10-fold cross-validation (CV) method is invited for the final validation.

A. Estimation Results of Machine Learning Methods

The results of the slip ratio estimation are studied in three aspects in this study, which are the input to the machine learning algorithm, the type of machine learning algorithm, and the working condition data used. First, the selection of the algorithm input term based on the previous data analysis section shows that the a_z and the slip ratio are the most distinctive ones, therefore, the a_z is used as the basis for this study with the combination of the other two directions, i.e., $a_x/a_y/a_z$, a_x/a_z , a_y/a_z and a_z , as the algorithm input to explore which input is the most valuable. Second, for verifying

TABLE II: SUMMARY OF TEST RESULTS ON DIFFERENT MACHINE LEARNING METHODS

Test condition	Testing dataset NRMS errors(%)				
	Estimation method	a_x, a_y, a_z	a_x, a_z	a_y, a_z	a_z
Data set 1	Neural network	2.62	3.13	2.77	2.17
	Gradient boosting machine	4.60	3.31	3.98	3.02
	Random forest	3.47	2.60	3.22	2.27
	Support vector machine	4.83	3.73	3.87	3.04
Data set 2	Neural network	3.56	2.78	3.56	3.87
	Gradient boosting machine	6.86	5.62	6.63	5.42
	Random forest	6.75	6.17	7.58	5.41
	Support vector machine	5.46	4.50	4.48	3.18
Data set 3	Neural network	11.08	10.16	9.59	17.50
	Gradient boosting machine	14.06	12.58	15.21	12.76
	Random forest	15.37	14.25	16.64	13.41
	Support vector machine	19.61	17.02	16.27	12.95
Data set 4	Neural network	10.21	5.61	7.64	6.01
	Gradient boosting machine	6.30	5.36	6.39	5.58
	Random forest	7.81	7.19	7.45	6.89
	Support vector machine	12.36	10.76	9.32	7.30

the contribution of machine learning algorithms combined with intelligent tires for slip ratio estimation, the validation of different algorithms is also carried out, where the algorithms include NN, GBM, RF and SVM. Furthermore, in order to distinguish the effects in estimation results due to working conditions, different sub-working conditions (Data set 1, Data set 2, Data set 3, and Data set 4) are also calculated separately.

TABLE II shows the normalized root mean square (NRMS) error statistics of the slip ratio for the three influencing factors mentioned above. The first factor, i.e. the algorithm input, which can be seen in conjunction with the information in Fig. 17, where the four inputs are distinguished by four different colors. It can be intuitively observed from Fig. 17 that regardless of which machine learning algorithm and any one class of dataset is used, a_z has the most excellent results, except for the NN which has abnormal estimation results in Data set 3. While the results of $a_x/a_y/a_z$ are relatively less satisfactory, the estimation results of a_x/a_z and a_y/a_z are similar. Second, in terms of different machine learning algorithms, NN performs well except for Data set 3 and Data set 4 with a_z as input, where the performance is worse. The next best performer is GBM, especially in Data set 4, where the estimation results are stable for all four inputs. The relatively poor performer is the SVM algorithm. Finally, the analysis is performed according to the estimation results of different datasets. Such as Data set 1 and Data set 2 with small slip ratio conditions, their NRMS errors are relatively smaller, the largest of which is the RF algorithm with a_y/a_z input in Data set 2, whose error is 7.58%, and the smallest is the NN algorithm with a_z input in Data set 1, whose error is 2.17%. In results Data set 3 with the large slip ratio, its NRMS error floats around 15% overall.

In addition to the numerical statistical results described

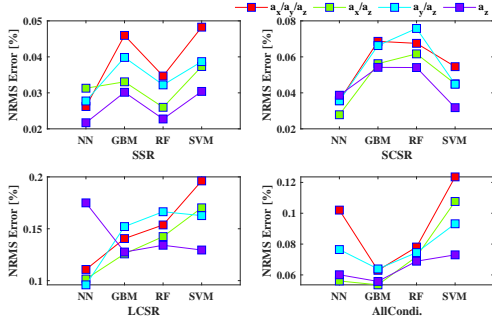


Fig. 17: Graphical representation of the NRMS error

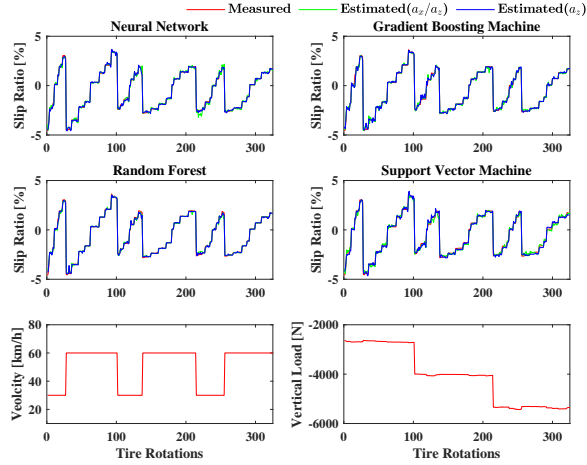


Fig. 18: Comparison of estimated slip ratio with different ML methods in Data set 1

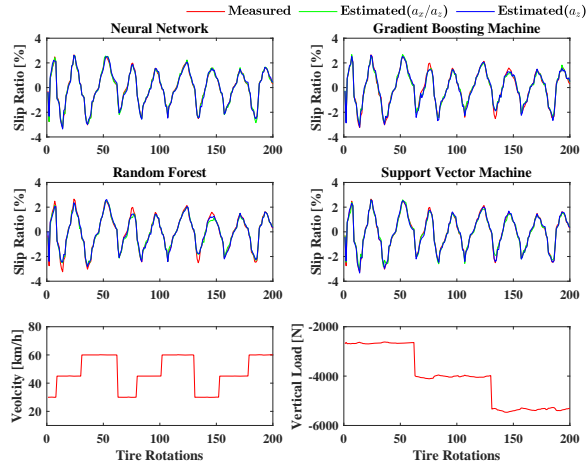


Fig. 19: Comparison of estimated slip ratio with different ML methods in Data set 2

above, two types of inputs, a_x/a_z and a_z , are selected for a more intuitive evaluation to graphically compare the estimated values with the measured values. As shown in Figs. 18-21, the estimated performances of the four datasets, i.e., Data set 1, Data set 2, Data set 3 and Data set 4, are presented respectively, where the different inputs are distinguished by color and the different algorithms are separated by subplot. In Fig. 18, estimation of results for all inputs in different

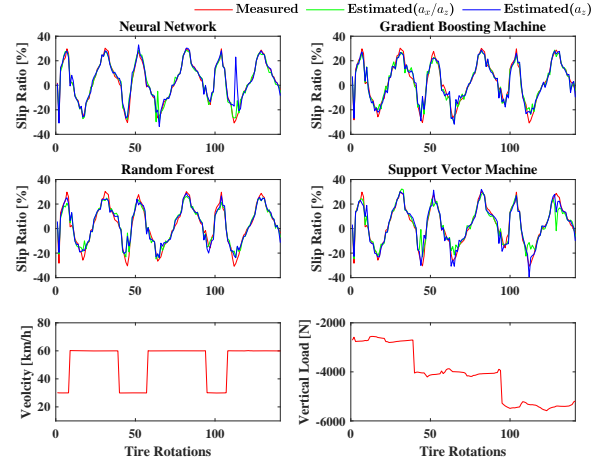


Fig. 20: Comparison of estimated slip ratio with different ML methods in Data set 3

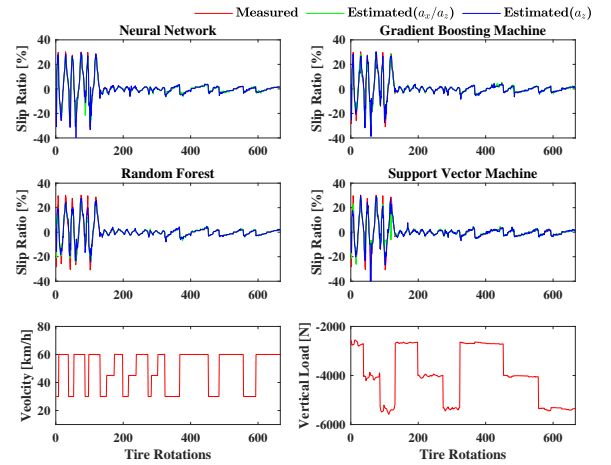


Fig. 21: Comparison of estimated slip ratio with different ML methods in Data set 4

machine learning methods are able to match well with the measured real values, with some robustness to both velocity and load. Similarly it can be observed in Fig. 19 that both inputs maintain good performance except in GBM and RF where the difference between measured and estimated values occurs at several points where the slip ratio is relatively large. It can also be examined from TABLE II that the NRMS errors are 5.62% and 6.17% for GBM and RF with a_x/a_z input, and 5.42% and 5.41% with a_z input, respectively. Next, the maximum slip ratio reaches 30% in Data set 3, and it is also obvious from Fig. 20 that the estimation error occurs at the large slip ratio (around 30%) regardless of the algorithm and input, but on the whole, NN has better results than the other algorithms. Meanwhile, it is worth noting that the estimation result of the NN algorithm with a_z as input in Fig. 20 shows a large error value at about the 120th sample point, which may be caused by problems with the characteristics of the a_z signal itself. Fig. 21 shows the overall estimation results of Data set 4, and it can be seen that the NN algorithm's results are closer to the measured values at large slip ratio, and the performance is more promising. Meanwhile, the larger error

that appears in Data set 3 disappears in this dataset.

B. 10-Folds Cross-Validation

To effectively test the performance of different machine learning algorithms on unknown data, an approach, k-fold cross-validation (CV), is recommended. It is to split the training set data into k subsamples, keep one as the model test set data, and the remaining k-1 subsamples are used to train the model. K-fold CV is repeated so that each subsample can be sufficiently utilized. And that method is usually the most commonly used.

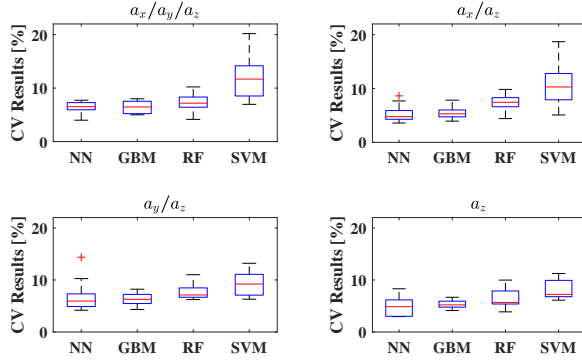


Fig. 22: Boxplot of CV results

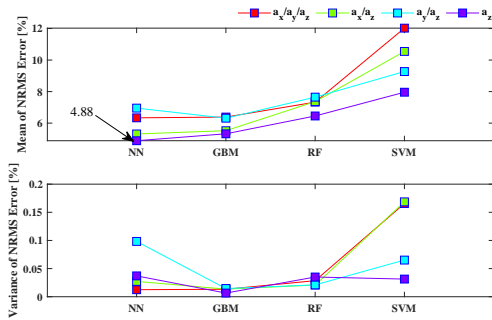


Fig. 23: Comparison of mean and variance for CV results

The dataset of Data set 4 contains all the data of the slip ratio variation type for this experiment, which is used to do the 10-fold CV more convincingly. Fig. 22 shows the boxplot for the CV of different machine learning algorithms for the four input types. Also more convenient for comparison between different factors, the mean and variance of the CV results are plotted in Fig. 23. It can be observed from the Fig. 23 that the smallest average value of NRMS errors is the NN algorithm model with a_z as input, which value is 4.88%. A more adequate analysis can be conducted in two aspects. First, considering the different algorithms separately, and combining the information in Figs. 22 and 23, GBM has a similar mean value to NN, a noteworthy case that the variance is smaller than NN's. From an overall perspective, GBM performs the best in general. NN has the lowest mean value, but the variance is less stable. In particular, outliers appear in the CV results for each of a_x/a_z and a_y/a_z as inputs in Fig. 22. Compared with SVM, RF has relatively small variance and average value,

which is better than the performance of SVM algorithm. From the algorithm itself is concerned, GBM's hyper-parameter more complex, NN followed the simplest, least parameters for RF and SVM. Second, observed with the four input results, the a_z input type performs better overall, with the smallest mean and relatively small variance, regardless of the algorithm. $a_x/a_y/a_z$ input results have a relatively poor performance in terms of mean value but the smallest variance. a_x/a_z and a_y/a_z inputs have very little difference in performance and are almost equal. This phenomenon can also be concluded from the previous data analysis section III, where the correlation between a_z features and the slip ratio is optimal and stable. Meanwhile, this means that there are fewer accelerations in two directions, allowing the algorithm to run with less data and reduce computational costs, which offers the possibility of real time operation of real vehicles in the future.

VI. CONCLUSION

In this thesis, an intelligent tire system is tested on the MTS tire test bench to acquire acceleration signals under different longitudinal slip conditions. Then, three directional acceleration (a_x , a_y , and a_z) in the tire contact patch are extracted for filtering and assembled into four types as inputs for the four machine learning algorithms. In order to evaluate the model performance of these machine learning algorithms, the 10-fold CV method is performed for each of them. From the NRMS error results of machine learning methods, the mean value of GBM is relatively small and has the minimum variance, indicating better stability but more complicated models. The mean value of NN is similar to GBM's but has an outlier with a_x/a_z and a_y/a_z input. Compared with RF, the mean and variance of SVM are relatively larger, but both models are more simple, so RF is more promising for application when compared to SVM. From the NRMS error results of the algorithms with different input types, the performance of a_z is more promising, and the NRMS error of the NN algorithm model is 4.88%. In summary, the utilization of data from intelligent tire systems combined with machine learning algorithms has a high potential in the field of tire slip ratio estimation. For future research work, we will extend more training samples (for different tire brands, tire pressures, and even combined working conditions) to prove the performance of the intelligent tire system for slip ratio estimation.

REFERENCES

- [1] A. Tæihagh and H. S. M. Lim, "Governing autonomous vehicles: emerging responses for safety, liability, privacy, cybersecurity, and industry risks," *Transport reviews*, vol. 39, no. 1, pp. 103–128, 2019.
- [2] A. Papadoulis, M. Qudus, and M. Imprialou, "Evaluating the safety impact of connected and autonomous vehicles on motorways," *Accident Analysis & Prevention*, vol. 124, pp. 12–22, 2019.
- [3] H. Heidfeld, M. Schünemann, and R. Kasper, "Ukf-based state and tire slip estimation for a 4wd electric vehicle," *Vehicle System Dynamics*, vol. 58, no. 10, pp. 1479–1496, 2020.
- [4] W.-Y. Wang, I.-H. Li, M.-C. Chen, S.-F. Su, and S.-B. Hsu, "Dynamic slip-ratio estimation and control of antilock braking systems using an observer-based direct adaptive fuzzy-neural controller," *IEEE Transactions on Industrial Electronics*, vol. 56, no. 5, pp. 1746–1756, 2008.
- [5] J. H. Park and C. Y. Kim, "Wheel slip control in traction control system for vehicle stability," *Vehicle system dynamics*, vol. 31, no. 4, pp. 263–278, 1999.

- [6] B.-R. Liang and W.-S. Lin, "A new slip ratio observer and its application in electric vehicle wheel slip control," in *2012 IEEE International Conference on Systems, Man, and Cybernetics (SMC)*. IEEE, 2012, pp. 41–46.
- [7] M. Boisvert and P. Micheau, "Estimators of wheel slip for electric vehicles using torque and encoder measurements," *Mechanical Systems and Signal Processing*, vol. 76, pp. 665–676, 2016.
- [8] X. Zhang, Y. Xu, M. Pan, and F. Ren, "A vehicle abs adaptive sliding-mode control algorithm based on the vehicle velocity estimation and tyre/road friction coefficient estimations," *Vehicle System Dynamics*, vol. 52, no. 4, pp. 475–503, 2014.
- [9] S. Seyedtabaai and A. Velayati, "Adaptive optimal slip ratio estimator for effective braking on a non-uniform condition road," *Automatika*, vol. 60, no. 4, pp. 413–421, 2019.
- [10] D. M. Bevil, J. Ryu, and J. C. Gerdes, "Integrating ins sensors with gps measurements for continuous estimation of vehicle sideslip, roll, and tire cornering stiffness," *IEEE Transactions on Intelligent Transportation Systems*, vol. 7, no. 4, pp. 483–493, 2006.
- [11] Y. Hori, Y. Toyoda, and Y. Tsuruoka, "Traction control of electric vehicle: basic experimental results using the test ev" uot electric march," *IEEE transactions on Industry Applications*, vol. 34, no. 5, pp. 1131–1138, 1998.
- [12] K. Fujii and H. Fujimoto, "Traction control based on slip ratio estimation without detecting vehicle speed for electric vehicle," in *2007 Power Conversion Conference-Nagoya*. IEEE, 2007, pp. 688–693.
- [13] M. Cecotti, J. Larminie, and B. Azzopardi, "Estimation of slip ratio and road characteristics by adding perturbation to the input torque," in *2012 IEEE International Conference on Vehicular Electronics and Safety (ICVES 2012)*. IEEE, 2012, pp. 31–36.
- [14] K. Maeda, H. Fujimoto, and Y. Hori, "Four-wheel driving-force distribution method based on driving stiffness and slip ratio estimation for electric vehicle with in-wheel motors," in *2012 IEEE Vehicle Power and Propulsion Conference*. IEEE, 2012, pp. 1286–1291.
- [15] T. Vo-Duy and M. C. Ta, "Slip ratio estimation for traction control of electric vehicles," in *2018 IEEE Vehicle Power and Propulsion Conference (VPPC)*. IEEE, 2018, pp. 1–6.
- [16] N. Xu, H. Askari, Y. Huang, J. Zhou, and A. Khajepour, "Tire force estimation in intelligent tires using machine learning," *IEEE Transactions on Intelligent Transportation Systems*, pp. 1–10, 2020.
- [17] N. Xu, Y. Huang, H. Askari, and Z. Tang, "Tire slip angle estimation based on the intelligent tire technology," *IEEE Transactions on Vehicular Technology*, vol. 70, no. 3, pp. 2239–2249, 2021.
- [18] D. Maurya, S. Khaleghian, R. Sriramdas, P. Kumar, R. A. Kishore, M. G. Kang, V. Kumar, H.-C. Song, S.-Y. Lee, Y. Yan *et al.*, "3d printed graphene-based self-powered strain sensors for smart tires in autonomous vehicles," *Nature communications*, vol. 11, no. 1, pp. 1–10, 2020.
- [19] D. Maurya, P. Kumar, S. Khaleghian, R. Sriramdas, M. G. Kang, R. A. Kishore, V. Kumar, H.-C. Song, J.-M. J. Park, S. Taheri *et al.*, "Energy harvesting and strain sensing in smart tire for next generation autonomous vehicles," *Applied energy*, vol. 232, pp. 312–322, 2018.
- [20] H. Askari, E. Hashemi, A. Khajepour, M. B. Khamesee, and Z. L. Wang, "Tire condition monitoring and intelligent tires using nanogenerators based on piezoelectric, electromagnetic, and triboelectric effects," *Advanced Materials Technologies*, vol. 4, no. 1, p. 1800105, 2019.
- [21] Askari, Hassan and Hashemi, Ehsan and Khajepour, Amir and Khamesee, Mir Behrad and Wang, Zhong Lin, "Towards self-powered sensing using nanogenerators for automotive systems," *Nano Energy*, vol. 53, pp. 1003–1019, 2018.
- [22] R. Matsuzaki and A. Todoroki, "Wireless flexible capacitive sensor based on ultra-flexible epoxy resin for strain measurement of automobile tires," *Sensors and Actuators A: Physical*, vol. 140, no. 1, pp. 32–42, 2007.
- [23] Matsuzaki, Ryosuke and Todoroki, Akira, "Passive wireless strain monitoring of actual tire using capacitance-resistance change and multiple spectral features," *Sensors and Actuators A: Physical*, vol. 126, no. 2, pp. 277–286, 2006.
- [24] F. Coppo, G. Pepe, N. Roveri, and A. Carcaterra, "A multisensing setup for the intelligent tire monitoring," *Sensors*, vol. 17, no. 3, p. 576, 2017.
- [25] N. Roveri, G. Pepe, and A. Carcaterra, "Optyre—a new technology for tire monitoring: Evidence of contact patch phenomena," *Mechanical Systems and Signal Processing*, vol. 66, pp. 793–810, 2016.
- [26] A. Pohl, R. Steindl, and L. Reindl, "The" intelligent tire" utilizing passive saw sensors measurement of tire friction," *IEEE transactions on instrumentation and measurement*, vol. 48, no. 6, pp. 1041–1046, 1999.
- [27] L. M. Reindl, A. Pohl, G. Scholl, and R. Weigel, "Saw-based radio sensor systems," *IEEE Sensors Journal*, vol. 1, no. 1, pp. 69–78, 2001.
- [28] O. Yilmazoglu, M. Brandt, J. Sigmund, E. Genc, and H. Hartnagel, "Integrated inas/gasb 3d magnetic field sensors for "the intelligent tire"," *Sensors and Actuators A: Physical*, vol. 94, no. 1-2, pp. 59–63, 2001.
- [29] A. J. Tuononen, "Optical position detection to measure tyre carcass deflections," *Vehicle System Dynamics*, vol. 46, no. 6, pp. 471–481, 2008.
- [30] V. Magori, V. R. Magori, and N. Seitz, "On-line determination of tyre deformation, a novel sensor principle," in *1998 IEEE Ultrasonics Symposium. Proceedings (Cat. No. 98CH36102)*, vol. 1. IEEE, 1998, pp. 485–488.
- [31] R. Matsuzaki, K. Kamai, and R. Seki, "Intelligent tires for identifying coefficient of friction of tire/road contact surfaces using three-axis accelerometer," *Smart Materials and Structures*, vol. 24, no. 2, p. 025010, 2014.
- [32] A. Niskanen and A. J. Tuononen, "Three three-axis iepe accelerometers on the inner liner of a tire for finding the tire-road friction potential indicators," *Sensors*, vol. 15, no. 8, pp. 19 251–19 263, 2015.
- [33] K. Guo and D. Lu, "Unitire: unified tire model for vehicle dynamic simulation," *Vehicle System Dynamics*, vol. 45, no. S1, pp. 79–99, 2007.
- [34] H. B. Pacejka and E. Bakker, "The magic formula tyre model," *Vehicle system dynamics*, vol. 21, no. S1, pp. 1–18, 1992.
- [35] H. Pacejka, *Tire and vehicle dynamics*. Elsevier, 2005.
- [36] H.-N. Robert *et al.*, "Theory of the backpropagation neural network," *Proc. 1989 IEEE IJCNN*, vol. 1, pp. 593–605, 1989.
- [37] J. H. Friedman, "Greedy function approximation: a gradient boosting machine," *Annals of statistics*, pp. 1189–1232, 2001.
- [38] T. K. Ho, "The random subspace method for constructing decision forests," *IEEE transactions on pattern analysis and machine intelligence*, vol. 20, no. 8, pp. 832–844, 1998.
- [39] W. S. Noble, "What is a support vector machine?" *Nature biotechnology*, vol. 24, no. 12, pp. 1565–1567, 2006.



Nan Xu received the Ph.D. degree in vehicle engineering from Jilin University, Changchun, China, in 2012. He is currently an associate professor at State Key Laboratory of Automotive Simulation and Control, Jilin University. His current research focuses on tire dynamics, intelligent tire, vehicle dynamics, stability control of electric vehicles and autonomous vehicles.



Zepeng Tang is currently a M.S. candidate in the College of Automotive Engineering, Jilin University, Changchun, China. His research interest is mainly on intelligent tire, vehicle dynamics and autonomous vehicles.



Jianfeng Zhou received his B.E. degree in automotive engineering in 2018 from Jinlin University, Changchun, China, where he is currently working toward the M.S. degree. His current research focuses on tire dynamics, intelligent tire and vehicle dynamics.



Hassan Askari was born in Rasht, Iran and received his B. Sc., M.Sc. and PhD degrees from Iran University of Science and Technology, Tehran, Iran, University of Ontario Institute of Technology, Oshawa, Canada, and University of Waterloo, Waterloo, Canada in 2011, 2014, and 2019 respectively. He published more than 70 journal and conference papers in the areas of nonlinear vibrations, applied mathematics, nanogenerators and self-powered sensors. He co-authored one book and one book chapter both published by Springer. He is an active reviewer

for more than 40 journals and editorial board member of several scientific and international journals. He has received several prestigious awards including, Outstanding Researcher at the Iran University of Science and Technology, Fellowship of the Waterloo Institute of Nanotechnology, NSERC Graduate Scholarship, Ontario Graduate Scholarship, and the University of Waterloo President Award. He was nominated for the Governor General's Academic Gold Medal at the University of Ontario Institute of Technology and University of Waterloo in 2014 and 2019, respectively. He is currently a Postdoctoral Fellow at the Department of Mechanical and Mechatronics Engineering at the University of Waterloo.